

# Joint Processing and Transmission Energy Optimization for ISAC in Cell-Free Massive MIMO with URLLC

Zinat Behdad\*, Özlem Tuğfe Demir<sup>†</sup>, Ki Won Sung\*, and Cicek Cavdar\*

\*Department of Computer Science, KTH Royal Institute of Technology, Stockholm, Sweden ({zinatb, sungkw, cavdar}@kth.se) <sup>†</sup>Department of Electrical-Electronics Engineering, TOBB ETU, Ankara, Turkey (ozlemtugfedemir@etu.edu.tr)

**Abstract**—In this paper, we explore the concept of integrated sensing and communication (ISAC) within a downlink cell-free massive MIMO (multiple-input multiple-output) system featuring multi-static sensing and users requiring ultra-reliable low-latency communications (URLLC). Our work focuses on devising two algorithms that concurrently optimize power and blocklength allocation. The objectives of these algorithms are to minimize the energy consumption solely for transmission and the overall end-to-end (E2E) energy consumption, which encompasses sensing/communication processing and transmission. This is achieved while meeting the necessary requirements for sensing and URLLC. To address the inherent non-convexity of these optimization problems, we apply feasible point pursuit - successive convex approximation (FPP-SCA), concave-convex programming (CCP), and fractional programming. Our numerical analysis compares the performance of these algorithms in ISAC scenarios and against a baseline URLLC-only scenario without sensing integration. Results show the E2E energy minimization algorithm's effectiveness, particularly in scenarios without sensing. Additionally, our study underscores the increasing prominence of energy consumption associated with sensing processing tasks as the number of sensing receive access points rises, indicating potential for energy savings by selectively deactivating APs. Furthermore, the results emphasize that although increasing the number of transmit APs can improve URLLC satisfaction and sensing update rate by reducing blocklength, careful management is essential to avoid excessive energy consumption and reduced detection probability.

**Index Terms**—Integrated sensing and communication, cell-free massive MIMO, URLLC, power allocation, blocklength

## I. INTRODUCTION

6G mobile networks are expected to offer various sensing-based applications such as autonomous vehicles, smart homes/cities/factories, remote healthcare, and location/environment-aware scenarios [1], [2]. Many of these applications, such as autonomous vehicles and industrial Internet-of-things (IIoT), demand ultra-reliable delivering of the sensing information to the user equipments (UEs) with a minimum reliability of 99.999% and within a low end-to-end (E2E) delay of less than 10-150 ms [3]–[5]. This demand necessitates two key aspects defined in 6G networks: integrated

sensing and communication (ISAC) together with ultra-reliable low-latency communication (URLLC). For most URLLC applications, short codewords are usually needed to satisfy latency constraints where codes with short blocklengths, e.g., 50-400 symbols are employed. Short blocklengths result in decoding errors; therefore, to ensure reliability, it is essential to consider the finite blocklength regime for modeling the decoding error probability (DEP) [6]–[8].

In mission-critical applications such as traffic control and autonomous vehicles, real-time transmission of sensing information to URLLC UEs is essential, as the speed of information updates directly impacts the effectiveness of these applications. In this paper, we introduce the concept of the “sensing update rate (SUR),” which quantifies the number of sensing measurements and updates per time unit [9]. The SUR is influenced by the blocklength, with longer blocklengths resulting in lower update rates due to the extended duration of each sensing operation. This dependency creates an opportunity to optimize blocklength to balance reliable communication with high SUR. Although URLLC and ISAC have typically been studied as separate domains, a joint design and optimization approach is required to meet the distinct requirements of both and maximize integration gains.

Cell-free massive multiple-input multiple-output (CF-mMIMO) has been shown to be a good candidate to facilitate stringent requirements of URLLC applications [8], [10], [11] as it provides high reliability by handling large path-loss variations and improves cell-edge user performance. CF-mMIMO can also facilitate ISAC implementations leveraging distributed access points (APs) to deploy bi-static/ multi-static sensing eliminating the need for full-duplex capability at the APs [12]–[15]. The central processing of network functions within a centralized radio access network (C-RAN) architecture facilitates coordination among distributed APs, enabling joint transmission and processing in CF-mMIMO [16]. C-RAN has evolved into virtualized C-RAN and, with the open interfaces, further into Open RAN (O-RAN), where virtualization enables the use of general-purpose servers for jointly processing of baseband and sensing signals.

However, deploying these technologies in 6G is anticipated to result in substantial energy consumption. In CF-mMIMO networks, baseband processing combined with sensing tasks is expected to lead to higher energy usage in ISAC networks

Results incorporated in this paper received funding from the ECSEL Joint Undertaking (JU) under grant agreement No 876124. The JU receives support from the EU Horizon 2020 research and innovation programme and Vinnova in Sweden. Ö. T. Demir was supported by 2232-B International Fellowship for Early Stage Researchers Programme funded by the Scientific and Technological Research Council of Türkiye.

compared to conventional communication systems. The impact of sensing on energy consumption in such networks has not been well-studied. Existing studies on green CF-mMIMO primarily focus on optimizing transmit power consumption in radio access, with limited work addressing processing energy, aside from [17]. Virtualized C-RAN architecture facilitates centralized processing and enables the sharing of processing resources between APs and tasks, paving the way for end-to-end (E2E) optimization of both processing and radio resources in ISAC networks. This motivates a comprehensive study of the E2E energy consumption in ISAC networks, considering not only energy consumption for transmission but also for processing tasks. The primary research question addressed in this paper is how to incorporate sensing in CF-mMIMO systems with URLLC while minimizing E2E energy consumption.

#### A. Literature Review

The finite blocklength regime and URLLC have primarily been studied in the context of cellular networks (see [18]–[20] and references therein), with limited research addressing URLLC in CF-mMIMO networks. The potentials of massive MIMO in meeting URLLC requirements for industrial automation are investigated in [21]–[23]. Network availability is investigated in [21] and [22], and [23] proposes a power allocation algorithm to maximize the minimum signal-to-interference-plus-noise ratio (SINR). The authors in [24] propose two power optimization algorithms to provide URLLC for traditional ground UEs and unmanned aerial vehicles (UAVs). The objectives in [24] are maximizing either sum or minimum URLLC rate and they study neither energy minimization nor blocklength optimization. Max-min rate optimization is also studied in [11], where the authors adapt a special class of the conjugate beamforming for a CF-mMIMO with single-antenna APs. Moreover, the authors aim to address an energy efficiency optimization problem.

Joint power and blocklength optimization is studied in [25] and [26] to optimize the reliability in a factory automation scenario and heterogeneous cellular networks, respectively. Cell-free networks as well as energy minimization are not studied in these works. Moreover, sensing requirements are not considered in [11], [21], [23]–[26].

There are few works that jointly consider URLLC and ISAC. In [5], a joint precoding scheme is proposed to minimize transmit power, satisfying sensing and delay requirements. Moreover, joint ISAC beamforming and scheduling design is addressed in [27] for periodic and aperiodic traffic.

The consideration of E2E energy-awareness has been explored in various contexts, as reflected in prior works such as [17], [28]–[31]. In particular, [30] studied fully virtualized E2E power minimization problem for CF-mMIMO on O-RAN architecture by taking the radio, fronthaul, and processing resources into account. Joint user scheduling and power allocation scheme for cell-free ISAC systems is studied in [32] that aims to maximize the sum-rate of the communication UEs and the sensing targets. However, the authors do not consider either URLLC requirements or energy minimization.

To the best of our knowledge, for the first time, ISAC in CF-mMIMO with URLLC UEs and with the focus on energy

efficiency was studied in our previous work [33]. In [33], we propose a successive convex approximation-based power allocation algorithm that maximizes energy efficiency while satisfying the sensing and URLLC requirements for a given blocklength. However, the impact of blocklength optimization is not considered in [33]. In this paper, we extend [33] from an E2E energy minimization perspective and aim to address a joint blocklength and power optimization problem. Here, E2E refers to considering energy consumption at both radio site and the central cloud.

#### B. Contributions

In this paper, we study E2E energy consumption in a CF-mMIMO system with URLLC UEs and multi-static sensing in a cluttered environment. We sense one candidate location of the target utilizing communication signals and an additional sensing signal. The sensing signals can cause interference for the UEs. Thus, we design the sensing precoding vectors to null the interference for the UEs. We consider a maximum DEP threshold, representing the reliability requirement, together with a maximum transmission delay threshold as the URLLC requirements and a minimum SINR as the sensing requirement. The latter is motivated by the fact that given a fixed false alarm probability, detection probability increases with a higher sensing SINR [34], [9, Chap. 3 and 15].

Different from [33], we conduct a comprehensive analysis of the processing requirements, specifically in terms of giga-operations per second (GOPS), and examine its impact on processing energy consumption. The main contributions of this paper are outlined as follows:

- We propose two joint blocklength and power allocation algorithms aimed at minimizing transmission energy consumption and E2E energy consumption, respectively, while satisfying URLLC and sensing requirements. To address the non-convex optimization challenges, we employ feasible point pursuit - successive convex approximation (FPP-SCA), concave-convex programming (CCP), and fractional programming.
- We analyze the impact of E2E energy minimization, covering both radio and processing energy consumption, within the proposed ISAC scenario and a comparative scenario that considers only URLLC requirements.
- We examine two distinct target detection schemes, comparing their performance in terms of E2E energy consumption, detection probability, and sensing update rate.
- We conduct sensitivity analyses to evaluate the effects of DEP threshold, sensing SINR threshold, and the number of ISAC transmit APs and sensing receive APs on E2E energy consumption, detection probability, and sensing update rate.

The rest of the paper is organized as follows: Section II introduces the system model. Section III provides URLLC analysis, considering DEP and delay in finite blocklength regime. Section IV covers the sensing analysis. Section V describes the E2E power model and derives GOPS analysis for both communication and sensing. Optimization problems are presented in Section VI, followed by numerical results and conclusions in Sections VII and VIII, respectively.

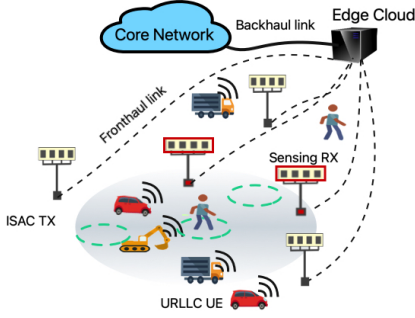


Fig. 1: Illustration of an ISAC system in CF-mMIMO with URLLC UEs.

## II. SYSTEM MODEL

We study ISAC in a CF-mMIMO system in URLLC scenarios. The system adopts a virtualized C-RAN architecture [35] for uplink channel estimation and downlink communication, as well as multi-static sensing as shown in Fig. 1. All the APs are interconnected via fronthaul links to the edge cloud and operate in full synchronization. We consider the original form of CF-mMIMO [8], wherein all the  $N_{\text{tx}}$  ISAC APs jointly serve the  $N_{\text{ue}}$  URLLC UEs by transmitting precoded signals containing both communication and sensing symbols.

Concurrently, the  $N_{\text{rx}}$  sensing receive APs engage in simultaneous sensing of the candidate location to detect the target. Each AP is equipped with an array of  $M$  antennas configured in a horizontal uniform linear array (ULA) with half-wavelength spacing. The respective array response vector is  $\mathbf{a}(\varphi, \vartheta) = [1 \ e^{j\pi \sin(\varphi) \cos(\vartheta)} \ \dots \ e^{j(M-1)\pi \sin(\varphi) \cos(\vartheta)}]^T$ , where  $\varphi$  and  $\vartheta$  are the azimuth and elevation angles from the AP to the target location, respectively [36].

We consider the finite blocklength regime for URLLC UEs, where a packet of  $b_i$  bits is sent to UE  $i$  within a transmission block with blocklength  $L = L_p + L_d$  symbols using the coherence bandwidth  $B$ .  $L_p$  and  $L_d$  are the number of symbols for pilot and data, respectively. It is expected that duration of each URLLC transmission, denoted by  $T$ , is shorter than one coherence time  $T_c$ , i.e.,  $T < T_c$  [11]. Without loss of generality, we assume that we have a channel estimation phase in each transmission.

### A. Downlink Communication

Let  $s_i[m]$  and  $s_0[m]$  represent the downlink communication symbol for UE  $i$  and sensing symbol, respectively at time instance  $m$ . The symbols are independent and have zero mean and unit power. Moreover, let  $\rho_i \geq 0$  and  $\rho_0 \geq 0$  be, respectively, the power control coefficients for UE  $i$  and the target, which are fixed throughout the transmission. Then, the transmitted signal from transmit AP  $k \in \{1, \dots, N_{\text{tx}}\}$  at time instance  $m$  is

$$\mathbf{x}_k[m] = \sum_{i=0}^{N_{\text{ue}}} \sqrt{\rho_i} \mathbf{w}_{i,k} s_i[m] = \mathbf{W}_k \mathbf{D}_s[m] \boldsymbol{\rho}, \quad (1)$$

where the vectors  $\mathbf{w}_{i,k} \in \mathbb{C}^M$  and  $\mathbf{w}_{0,k} \in \mathbb{C}^M$  are the transmit precoding vectors for transmit AP  $k$  corresponding to UE  $i$  and the sensing signal, respectively. In (1),  $\mathbf{W}_k = [\mathbf{w}_{0,k} \ \mathbf{w}_{1,k} \ \dots \ \mathbf{w}_{N_{\text{ue}},k}]$ ,  $\mathbf{D}_s[m] =$

$\text{diag}(s_0[m], s_1[m], \dots, s_{N_{\text{ue}}}[m])$  is the diagonal matrix containing the sensing and communication symbols, and  $\boldsymbol{\rho} = [\sqrt{\rho_0} \ \dots \ \sqrt{\rho_{N_{\text{ue}}}}]^T$ .

The communication channels are modeled as spatially correlated Rician fading which are assumed to remain constant during each coherence block, and the channel realizations are independent of each other. Let  $\mathbf{h}_{i,k} \in \mathbb{C}^M$  denote the channel between ISAC AP  $k$  and UE  $i$ , modeled as

$$\mathbf{h}_{i,k} = e^{j\varphi_{i,k}} \bar{\mathbf{h}}_{i,k} + \tilde{\mathbf{h}}_{i,k}, \quad (2)$$

which consists of a semi-deterministic line-of-sight (LOS) path, represented by  $e^{j\varphi_{i,k}} \bar{\mathbf{h}}_{i,k}$  with unknown phase-shift  $\varphi_{i,k} \sim \mathcal{U}[0, 2\pi)$ , i.e., uniformly distributed on  $[0, 2\pi)$ , and a stochastic non-LOS (NLOS) component  $\tilde{\mathbf{h}}_{i,k} \sim \mathcal{CN}(\mathbf{0}, \mathbf{R}_{i,k})$  with the spatial correlation matrix  $\mathbf{R}_{i,k} \in \mathbb{C}^{M \times M}$ . Both  $\bar{\mathbf{h}}_{i,k}$  and  $\mathbf{R}_{i,k}$  include the combined effect of geometric path loss and shadowing. We concatenate the channel vector  $\mathbf{h}_{i,k}$  in the collective channel vector

$$\mathbf{h}_i = [\mathbf{h}_{i,1}^T \ \dots \ \mathbf{h}_{i,N_{\text{tx}}}^T]^T \in \mathbb{C}^{N_{\text{tx}}M}, \quad (3)$$

for UE  $i$ . The received signal at UE  $i$  is given as

$$y_i[m] = \underbrace{\sqrt{\rho_i} \mathbf{h}_i^H \mathbf{w}_i s_i[m]}_{\text{Desired signal}} + \underbrace{\sum_{j=1, j \neq i}^{N_{\text{ue}}} \sqrt{\rho_j} \mathbf{h}_i^H \mathbf{w}_j s_j[m]}_{\text{Interference signal due to the other UEs}} + \underbrace{\sqrt{\rho_0} \mathbf{h}_i^H \mathbf{w}_0 s_0[m]}_{\text{Interference signal due to the sensing}} + \underbrace{n_i[m]}_{\text{Noise}}, \quad (4)$$

where  $n_i[m] \sim \mathcal{CN}(0, \sigma_n^2)$  is the independent receiver noise at UE  $i$  at time instance  $m$  and the collective precoding vectors

$$\mathbf{w}_i = [\mathbf{w}_{i,1}^T \ \mathbf{w}_{i,2}^T \ \dots \ \mathbf{w}_{i,N_{\text{tx}}}^T]^T \in \mathbb{C}^{N_{\text{tx}}M}, \quad (5)$$

for  $i = 1, \dots, N_{\text{ue}}$ , and

$$\mathbf{w}_0 = [\mathbf{w}_{0,1}^T \ \mathbf{w}_{0,2}^T \ \dots \ \mathbf{w}_{0,N_{\text{tx}}}^T]^T \in \mathbb{C}^{N_{\text{tx}}M}, \quad (6)$$

are the centralized precoding vectors.

Using the independence of the data and sensing signals, the average transmit power for transmit AP  $k \in \{1, \dots, N_{\text{tx}}\}$  is

$$P_k = \sum_{i=0}^{N_{\text{ue}}} \rho_i \mathbb{E} \{ \|\mathbf{w}_{i,k}\|^2 \}, \quad k = 1, \dots, N_{\text{tx}} \quad (7)$$

which should not exceed the maximum power limit  $P_{\text{tx}}$ .

In the subsequent section, we will present the specifics of the linear minimum mean-squared error (LMMSE)-based channel estimation.

### B. LMMSE-Based Channel Estimation

Within the URLLC transmission time comprising  $L$  symbols,  $L_p < L$  symbols are allocated for pilot transmission. A collection of  $L_p$  mutually orthogonal pilot sequences is represented by  $\phi_1, \dots, \phi_{L_p} \in \mathbb{C}^{L_p}$ , where  $\|\phi_t\|^2 = L_p$  for  $t = 1, \dots, L_p$ . These pilot sequences are assigned to the  $N_{\text{ue}}$  UEs. If the number of pilot sequences is less than the number of UEs (i.e.,  $L_p < N_{\text{ue}}$ ), then each pilot sequence may be assigned to multiple UEs. Let  $t_i \in \{1, \dots, L_p\}$  denote the index of the pilot sequence that is assigned to UE  $i$  and we

define  $\mathcal{P}_i = \{j \in \{1, \dots, N_{\text{ue}}\} | t_j = t_i\}$  as the set of UEs that share the same pilot with UE  $i$ .

The received signal at the ISAC AP  $k$  during the entire pilot transmission is denoted by  $\mathbf{Y}_k^p \in \mathbb{C}^{M \times L_p}$  where

$$\mathbf{Y}_k^p = \sum_{i=1}^{N_{\text{ue}}} \sqrt{\eta_i} \mathbf{h}_{i,k} \phi_{t_i}^T + \mathbf{N}_k, \quad (8)$$

where  $\eta_i > 0$  is the transmit power by UE  $i$  and  $\mathbf{N}_k \in \mathbb{C}^{M \times L_p}$  is the received noise at AP  $k$  with independent and identically distributed (i.i.d.)  $\mathcal{CN}(0, \sigma_n^2)$  entries. We assume that  $\bar{\mathbf{h}}_{i,k}$  and  $\mathbf{R}_{i,k}$ , representing the long-term statistics for the channel in (2), are known while the random phase-shift  $\varphi_{i,k}$  is unknown. With respect to estimating  $\mathbf{h}_{i,k}$ , let us form  $\mathbf{y}_{t_i,k}^p = \mathbf{Y}_k^p \phi_{t_i}^* \in \mathbb{C}^M$ , where

$$\mathbf{y}_{t_i,k}^p = \underbrace{\sqrt{\eta_i} L_p \mathbf{h}_{i,k}}_{\text{Desired part}} + \underbrace{\sum_{j \in \mathcal{P}_i \setminus \{i\}} \sqrt{\eta_j} L_p \mathbf{h}_{j,k}}_{\text{Interference part}} + \underbrace{\mathbf{n}_{t_i,k}}_{\text{Noise}}, \quad (9)$$

where  $\mathbf{n}_{t_i,k} = \mathbf{N}_k \phi_{t_i}^* \sim \mathcal{CN}(\mathbf{0}, \sigma_n^2 L_p \mathbf{I}_M)$ . If the number of UEs is greater than the number of mutually orthogonal pilot sequences, then each pilot sequence may be assigned to multiple UEs using the pilot assignment algorithm in [35, Alg. 4.1]. The LMMSE estimate of  $\mathbf{h}_{i,k}$  is given by [37]

$$\hat{\mathbf{h}}_{i,k} = \sqrt{\eta_i} \mathbf{R}'_{i,k} (\boldsymbol{\Psi}'_{t_i,k})^{-1} \mathbf{y}_{t_i,k}^p, \quad (10)$$

where  $\mathbf{R}'_{i,k}$  and  $\boldsymbol{\Psi}'_{t_i,k}$  are the spatial correlation matrix corresponding to channel  $\mathbf{h}_{i,k}$  and the correlation matrix of the received signal, respectively, given by

$$\mathbf{R}'_{i,k} \triangleq \mathbf{R}_{i,k} + \bar{\mathbf{h}}_{i,k} \bar{\mathbf{h}}_{i,k}^H \quad (11)$$

$$\boldsymbol{\Psi}'_{t_i,k} \triangleq \sum_{j \in \mathcal{P}_i} \eta_j L_p \mathbf{R}'_{j,k} + \sigma_n^2 \mathbf{I}_M. \quad (12)$$

It is worth noting that deriving MMSE channel estimation proves challenging due to the non-Gaussian distribution of channels resulting from random phase-shifts in the LOS paths. For the sake of tractability, we adhere to the use of LMMSE-based channel estimation in this paper.

### C. Multi-Static Sensing

We investigate multi-static sensing, involving multiple transmit and receive APs in the network. The network engages in target location sensing during the downlink phase. We assume the existence of a LOS connection between the target location and each transmit/receive AP.

In the presence of the target, each receive AP captures both the reflected signals from the target and undesired signals, referred to as clutter. The clutter, being independent of the target's presence, is treated as interference for sensing purposes. Without loss of generality, we assume that the LOS paths between transmit and receive APs are known and can be effectively canceled out. Consequently, the interference signals correspond to the reflected paths through obstacles and are henceforth denoted as target-free channels.

Let  $\mathbf{H}_{r,k} \in \mathbb{C}^{M \times M}$  denote the target-free channel matrix between transmit AP  $k$  and receive AP  $r$ . We use the correlated

Rayleigh fading model for the NLOS channels  $\mathbf{H}_{r,k}$ , which is modeled using the Kronecker model [38]. We define the random matrix  $\mathbf{W}_{\text{ch},(r,k)} \in \mathbb{C}^{M \times M}$  with i.i.d. entries with  $\mathcal{CN}(0, 1)$  distribution. The matrix  $\mathbf{R}_{\text{rx},(r,k)} \in \mathbb{C}^{M \times M}$  represents the spatial correlation matrix corresponding to receive AP  $r$  and with respect to the direction of transmit AP  $k$ . Similarly,  $\mathbf{R}_{\text{tx},(r,k)} \in \mathbb{C}^{M \times M}$  is the spatial correlation matrix corresponding to transmit AP  $k$  and with respect to the direction of receive AP  $r$ . The channel  $\mathbf{H}_{r,k}$  is written as

$$\mathbf{H}_{r,k} = \mathbf{R}_{\text{rx},(r,k)}^{\frac{1}{2}} \mathbf{W}_{\text{ch},(r,k)} \left( \mathbf{R}_{\text{tx},(r,k)}^{\frac{1}{2}} \right)^T, \quad (13)$$

where the channel gain is determined by the geometric path loss and shadowing, and is included in the spatial correlation matrices. The received signal at AP  $r$  in the presence of the target and for  $m \in \{1, \dots, L_d\}$ , can be formulated as

$$\mathbf{y}_r[m] = \sum_{k=1}^{N_{\text{tx}}} \underbrace{\alpha_{r,k} \sqrt{\beta_{r,k}} \mathbf{a}(\phi_r, \theta_r) \mathbf{a}^T(\varphi_k, \vartheta_k) \mathbf{x}_k[m]}_{\text{desired reflections from the target}} + \sum_{k=1}^{N_{\text{tx}}} \underbrace{\mathbf{H}_{r,k} \mathbf{x}_k[m]}_{\text{undesired signals}} + \mathbf{n}_r[m], \quad (14)$$

where  $\mathbf{n}_r[m] \sim \mathcal{CN}(\mathbf{0}, \sigma_n^2 \mathbf{I}_M)$  is the receiver noise at the  $M$  antennas of receive AP  $r$ . The second term in (14) acts as interference for the target detection. Here,  $\beta_{r,k}$  is the channel gain including the path-loss from transmit AP  $k$  to receive AP  $r$  through the target and the variance of bi-static radar cross-section (RCS) of the target denoted by  $\sigma_{\text{RCS}}$ . The  $\alpha_{r,k} \sim \mathcal{CN}(0, 1)$  is the normalized RCS of the target for the respective path. We assume the RCS values are i.i.d. and follow the Swerling-I model, meaning that they are constant throughout the consecutive  $L_d$  symbols collected for sensing [9].

Following the same notation as in [34], in (14), the known part of each reflected path is denoted by  $\mathbf{g}_{r,k}[m] \in \mathbb{C}^M$ , defined as

$$\mathbf{g}_{r,k}[m] \triangleq \sqrt{\beta_{r,k}} \mathbf{a}(\phi_r, \theta_r) \mathbf{a}^T(\varphi_k, \vartheta_k) \mathbf{x}_k[m], \quad (15)$$

where the matrix  $\alpha_{r,k} \sqrt{\beta_{r,k}} \mathbf{a}(\phi_r, \theta_r) \mathbf{a}^T(\varphi_k, \vartheta_k)$  represents the reflected path through the target. Here,  $\phi_r$  and  $\theta_r$  denote the azimuth and elevation angles from the target location to receiver AP  $r$ , respectively. Similarly,  $\varphi_k$  and  $\vartheta_k$  represent the azimuth and elevation angles from transmit AP  $k$  to the target location.

Each receive AP sends their respective signals  $\mathbf{y}_r[m]$ , for  $r = 1, \dots, N_{\text{rx}}$ , to the edge cloud, to form the collective received signal  $\mathbf{y}[m] = [\mathbf{y}_1^T[m] \ \dots \ \mathbf{y}_{N_{\text{rx}}}^T[m]]^T$ , which can be expressed as

$$\mathbf{y}[m] = \underbrace{\text{blkdiag}(\mathbf{G}_1[m], \dots, \mathbf{G}_{N_{\text{rx}}}[m])}_{\triangleq \mathbf{G}[m]} \boldsymbol{\alpha} + \underbrace{(\mathbf{I}_{N_{\text{rx}}} \otimes (\mathbf{x}^T[m] \otimes \mathbf{I}_M))}_{\triangleq \mathbf{X}[m]} \mathbf{h} + \mathbf{n}[m], \quad (16)$$

where  $\mathbf{G}_r[m] = [\mathbf{g}_{r,1}[m] \ \dots \ \mathbf{g}_{r,N_{\text{tx}}}[m]] \in \mathbb{C}^{M \times N_{\text{tx}}}$ ,  $\mathbf{x}[m] = [\mathbf{x}_1^T[m] \ \dots \ \mathbf{x}_{N_{\text{tx}}}^T[m]]^T \in \mathbb{C}^{N_{\text{tx}} M}$ , and  $\mathbf{h} \sim \mathcal{CN}(\mathbf{0}, \mathbf{R})$  is the vectorized target-free channels [34, Sec. V].

#### D. Target Detection

We employ two maximum a posteriori ratio test (MAPRT) detectors with two levels of complexity: the clutter-unaware detector [13] and the clutter-aware detector [34, Lem. 2]. The clutter-unaware detector ignores the presence of clutter for the sake of complexity reduction, whereas the clutter-aware detector accounts for unknown clutter. The corresponding test statistics are given by

$$T_{\text{c-unaware}} = \mathbf{a}^H \mathbf{C}^{-1} \mathbf{a}, \quad (17)$$

$$T_{\text{c-aware}} = \begin{bmatrix} \mathbf{a} \\ \mathbf{b} \end{bmatrix}^H \left( \begin{bmatrix} \mathbf{C} & \mathbf{E} \\ \mathbf{E}^H & \mathbf{D} \end{bmatrix}^{-1} - \begin{bmatrix} \mathbf{0} & \mathbf{0} \\ \mathbf{0} & \mathbf{D}^{-1} \end{bmatrix} \right) \begin{bmatrix} \mathbf{a} \\ \mathbf{b} \end{bmatrix}, \quad (18)$$

respectively, where

$$\mathbf{a} = \sum_{m=1}^{L_d} \mathbf{G}^H [m] \mathbf{y} [m], \quad \mathbf{b} = \sum_{m=1}^{L_d} \mathbf{X}^H [m] \mathbf{y} [m], \quad (19)$$

$$\mathbf{C} = \sum_{m=1}^{L_d} \mathbf{G}^H [m] \mathbf{G} [m] + \sigma_n^2 \mathbf{I}_{N_{\text{rx}} N_{\text{tx}}}, \quad (20)$$

$$\mathbf{D} = \sum_{m=1}^{L_d} \mathbf{X}^H [m] \mathbf{X} [m] + \sigma_n^2 \mathbf{R}^{-1}, \quad (21)$$

$$\mathbf{E} = \sum_{m=1}^{L_d} \mathbf{G}^H [m] \mathbf{X} [m]. \quad (22)$$

#### E. Transmit ISAC Precoding Vectors

The communication and sensing transmit precoding vectors are obtained based on regularized zero forcing (RZF) and zero forcing (ZF) approaches, respectively. The unit-norm RZF precoding vector for UE  $i$  is given as  $\mathbf{w}_i = \frac{\bar{\mathbf{w}}_i}{\|\bar{\mathbf{w}}_i\|}$ , with

$$\bar{\mathbf{w}}_i = \left( \sum_{j=1}^{N_{\text{ue}}} \hat{\mathbf{h}}_j \hat{\mathbf{h}}_j^H + \delta \mathbf{I}_{N_{\text{tx}} M} \right)^{-1} \hat{\mathbf{h}}_i, \quad i = 1, \dots, N_{\text{ue}}, \quad (23)$$

where  $\delta$  is the regularization parameter, and  $\hat{\mathbf{h}}_j = [\hat{\mathbf{h}}_{j,1}^T \dots \hat{\mathbf{h}}_{j,N_{\text{tx}}}^T]^T \in \mathbb{C}^{N_{\text{tx}} M}$  is the LMMSE channel estimate of the communication channel  $\mathbf{h}_j$ .

We aim to null the destructive interference from the sensing signal to the UEs by using the unit-norm ZF sensing precoding vector  $\mathbf{w}_0 = \frac{\bar{\mathbf{w}}_0}{\|\bar{\mathbf{w}}_0\|}$ , where

$$\bar{\mathbf{w}}_0 = (\mathbf{I}_{N_{\text{tx}} M} - \mathbf{U} \mathbf{U}^H) \mathbf{h}_0, \quad (24)$$

and  $\mathbf{U}$  is the unitary matrix with the orthogonal columns that span the column space of the matrix  $[\hat{\mathbf{h}}_1 \dots \hat{\mathbf{h}}_{N_{\text{ue}}}]$ .  $\mathbf{h}_0 = [\sqrt{\beta_1} \mathbf{a}^T(\varphi_1, \vartheta_1) \dots \sqrt{\beta_{N_{\text{tx}}}} \mathbf{a}^T(\varphi_{N_{\text{tx}}}, \vartheta_{N_{\text{tx}}})]^T \in \mathbb{C}^{N_{\text{tx}} M}$  is the concatenated sensing channel between all the ISAC APs and the target, including corresponding path loss and the array response vectors  $\mathbf{a}(\varphi_k, \vartheta_k)$  for  $k = 1, \dots, N_{\text{tx}}$ .

### III. RELIABILITY AND DELAY ANALYSIS FOR URLLC

In this section, we derive an upper bound on the DEP and the transmission delay, both crucial aspects considered as URLLC requirements. In the finite blocklength regime, the

communication data cannot be transmitted without error. From [10], ergodic data rate of UE  $i$  can be approximated as

$$R_i \approx \mathbb{E} \left\{ (1-\beta) \log_2 \left( 1 + \text{SINR}_i^{(\text{dl})} \right) - \frac{Q^{-1}(\epsilon_i)}{\ln(2)} \sqrt{\frac{(1-\beta)V_i}{L}} \right\}, \quad (25)$$

where  $\beta = \frac{L_p}{L}$ ,  $\epsilon_i$  denotes the DEP when transmitting  $b_i$  bits to UE  $i$ ,  $\text{SINR}_i^{(\text{dl})}$  is the instantaneous downlink communication signal-to-interference-plus-noise ratio (SINR) for UE  $i$ ,  $V_i = 1 - \left( 1 + \text{SINR}_i^{(\text{dl})} \right)^{-2}$  is the channel dispersion, and  $Q(\cdot)$  refers to the Gaussian Q-function. Due to the fact that  $V_i < 1$ , the ergodic data rate can be lower bounded by

$$R_i \geq (1-\beta) \mathbb{E} \left\{ \log_2 \left( 1 + \text{SINR}_i^{(\text{dl})} \right) \right\} - \frac{Q^{-1}(\epsilon_i)}{\ln(2)} \sqrt{\frac{(1-\beta)}{L}}. \quad (26)$$

Moreover, given that only  $\mathbb{E} \{ \mathbf{h}_i^H \mathbf{w}_i \}$  is known at UE  $i$ , and according to [35, Thm. 6.1] and [34, Lem. 1],

$$\mathbb{E} \left\{ \log_2 \left( 1 + \text{SINR}_i^{(\text{dl})} \right) \right\} \geq \log_2 \left( 1 + \overline{\text{SINR}}_i^{(\text{dl})} \right) \quad (27)$$

where

$$\overline{\text{SINR}}_i^{(\text{dl})} = \frac{\rho_i \mathbf{b}_i^2}{\sum_{j=0}^{N_{\text{ue}}} \rho_j \mathbf{a}_{i,j}^2 + \sigma_n^2}, \quad i = 1, \dots, N_{\text{ue}} \quad (28)$$

with

$$\mathbf{b}_i = |\mathbb{E} \{ \mathbf{h}_i^H \mathbf{w}_i \}|, \quad \mathbf{a}_{i,i} = \sqrt{\mathbb{E} \{ |\mathbf{h}_i^H \mathbf{w}_i|^2 \} - \mathbf{b}_i^2} \quad (29)$$

$$\mathbf{a}_{i,j} = \sqrt{\mathbb{E} \{ |\mathbf{h}_i^H \mathbf{w}_j|^2 \}}, \quad j = 0, 1, \dots, N_{\text{ue}}, \quad j \neq i. \quad (30)$$

The expectations are taken with respect to the random channel realizations. Now, using (27) and substituting  $R_i = \frac{b_i}{L}$  into (26), we obtain an upper bound for the DEP as

$$\epsilon_i \leq \epsilon_i^{(\text{ub})} \triangleq Q \left( \sqrt{L - L_p} \left[ \ln \left( 1 + \overline{\text{SINR}}_i^{(\text{dl})} \right) - \frac{b_i \ln 2}{L - L_p} \right] \right). \quad (31)$$

In this paper, we focus on the transmission delay and leave the analysis of E2E delay as future work. Let  $D_i^t$  denote the transmission delay of UE  $i$ , expressed as

$$D_i^t = \frac{T}{1 - \epsilon_i} = \frac{L}{B(1 - \epsilon_i)}, \quad i = 1, \dots, N_{\text{ue}} \quad (32)$$

where  $T = \frac{L}{B}$  is the time duration of one URLLC transmission with blocklength  $L$ . To satisfy the reliability requirement,  $\epsilon_i$  should be less than the maximum tolerable DEP denoted by  $\epsilon_i^{(\text{th})}$ . Then, since  $\epsilon_i \leq \epsilon_i^{(\text{ub})} \leq \epsilon_i^{(\text{th})}$ , the transmission delay is upper-bounded as

$$D_i^t \leq \frac{L}{B(1 - \epsilon_i^{(\text{th})})} \triangleq D_i^{(\text{ub})} \leq D_i^{(\text{th})}, \quad (33)$$

where  $D_i^{(\text{th})}$  is the maximum tolerable delay by UE  $i$  and  $D_i^{(\text{ub})} \leq D_i^{(\text{th})}$  should be satisfied to guarantee the delay requirement. This implies that the blocklength cannot exceed  $D_i^{(\text{th})} B(1 - \epsilon_i^{(\text{th})})$ . Thus, we can define the maximum tolerable blocklength by  $L_{\text{max}}$ , where

$$L_{\text{max}} = \min \left\{ D_i^{(\text{th})} B(1 - \epsilon_i^{(\text{th})}) \mid i = 1, \dots, N_{\text{ue}} \right\}. \quad (34)$$

#### IV. SENSING ANALYSIS

We assess the sensing performance in terms of detection probability under a certain false alarm probability and sensing update rate in terms of the number of sensing measurement updates per time unit. It is numerically shown in [13] and [34], that maximizing the sensing SINR improves the target detection probability under a constant false alarm probability. When studying other sensing tasks, it is naturally desired to keep the sensing SINR above a required threshold denoted by  $\gamma_s$ , i.e.,  $\text{SINR}_s \geq \gamma_s$ . This fact motivates the optimization problems presented in Section VI. In the following subsections, we present sensing SINR and sensing update rate.

##### A. Sensing SINR

From [34], the sensing SINR is given by

$$\text{SINR}_s = \frac{\boldsymbol{\rho}^T \mathbf{A} \boldsymbol{\rho}}{L_d M N_{\text{rx}} \sigma_n^2 + \boldsymbol{\rho}^T \mathbf{B} \boldsymbol{\rho}}, \quad (35)$$

where  $\boldsymbol{\rho} = [\sqrt{\rho_0} \dots \sqrt{\rho_{N_{\text{ue}}}}]^T$  and

$$\mathbf{A} = M \sum_{m=1}^{L_d} \mathbf{D}_s^H[m] \left( \sum_{r=1}^{N_{\text{rx}}} \sum_{k=1}^{N_{\text{tx}}} \beta_{r,k} \mathbf{W}_k^H \mathbf{a}^*(\varphi_k, \vartheta_k) \mathbf{a}^T(\varphi_k, \vartheta_k) \times \mathbf{W}_k \right) \mathbf{D}_s[m], \quad (36)$$

$$\mathbf{B} = \sum_{m=1}^{L_d} \mathbf{D}_s^H[m] \left( \sum_{r=1}^{N_{\text{rx}}} \sum_{k=1}^{N_{\text{tx}}} \text{tr}(\mathbf{R}_{\text{rx},(r,k)}) \mathbf{W}_k^H \mathbf{R}_{\text{tx},(r,k)}^T \mathbf{W}_k \right) \times \mathbf{D}_s[m]. \quad (37)$$

The sensing SINR is a function of symbols, which vary randomly for different blocklength values. This implies that although the symbols are known when processing the received sensing signals, they cannot be known during the resource allocation phase. To this end, we take the expectation with respect to the random symbols. Thus, the average sensing SINR would be

$$\overline{\text{SINR}}_s = \frac{M \boldsymbol{\rho}^T \mathbf{A}_D \boldsymbol{\rho}}{M N_{\text{rx}} \sigma_n^2 + \boldsymbol{\rho}^T \mathbf{B}_D \boldsymbol{\rho}}, \quad (38)$$

where  $\mathbf{A}_D$  and  $\mathbf{B}_D$  are diagonal matrices with

$$[\mathbf{A}_D]_{ii} = \sum_{r=1}^{N_{\text{rx}}} \sum_{k=1}^{N_{\text{tx}}} \beta_{r,k} (\mathbf{W}_k^H \mathbf{a}^*(\varphi_k, \vartheta_k) \mathbf{a}^T(\varphi_k, \vartheta_k) \mathbf{W}_k)_{ii}, \quad (39)$$

$$[\mathbf{B}_D]_{ii} = \sum_{r=1}^{N_{\text{rx}}} \sum_{k=1}^{N_{\text{tx}}} \text{tr}(\mathbf{R}_{\text{rx},(r,k)}) (\mathbf{W}_k^H \mathbf{R}_{\text{tx},(r,k)}^T \mathbf{W}_k)_{ii}. \quad (40)$$

##### B. Sensing Update Rate (SUR)

In our system model, the sensing information is updated once throughout each transmission block. Thus, the sensing update rate, denoted as  $R_s$ , is

$$R_s = \frac{B}{L} \quad (\text{updates/second}). \quad (41)$$

#### V. E2E POWER CONSUMPTION MODELING

Compared to communication networks, ISAC networks are expected to consume more power due to sensing tasks. In general, E2E power consumption in a system with virtualized C-RAN architecture is consisting of two main components: i) the radio site power consumption, including the AP power consumption and ii) the power consumption at the edge cloud, denoted by  $P_{\text{cloud}}$  [17].

In the considered virtualized C-RAN architecture, all processing is done in the cloud. Let  $P_{\text{AP},0}^{\text{tx}}$  and  $P_{\text{AP},0}^{\text{rx}}$  be the static power consumption of the transmit ISAC AP and the receive sensing AP, respectively. The total power consumption, taking into account both communication and sensing, can be expressed as

$$P_{\text{total}} = \underbrace{\sum_{k=1}^{N_{\text{tx}}} (P_{\text{AP},0}^{\text{tx}} + \Delta^{\text{tr}} P_k)}_{\text{radio site power consumption}} + \sum_{r=1}^{N_{\text{rx}}} P_{\text{AP},0}^{\text{rx}} + P_{\text{cloud}} \quad (42)$$

where  $\Delta^{\text{tr}}$  is the slope of load-dependent transmission power consumption of each AP. The  $P_k$  is the transmission power of the ISAC AP  $k$  from (7). The power consumption at the cloud is modeled as

$$P_{\text{cloud}} = P_{\text{fixed}} + \frac{1}{\sigma_{\text{cool}}} \left( P_{\text{cloud},0}^{\text{proc}} + \Delta_{\text{cloud}}^{\text{proc}} \frac{C_{\text{cloud}}}{C_{\text{max}}} \right), \quad (43)$$

where  $P_{\text{fixed}}$  is the fixed power consumption at the cloud which is independent of the load.  $P_{\text{cloud},0}^{\text{proc}}$  is the processing power consumption in the idle mode.  $\sigma_{\text{cool}} \in (0, 1]$  and  $\Delta_{\text{cloud}}^{\text{proc}}$  denote the cooling efficiency of the cloud and the slope of the load-dependent power consumption for processing at the digital unit (DU) in the cloud, respectively. Moreover,  $C_{\text{max}}$  and  $C_{\text{cloud}} \in [0, C_{\text{max}}]$  are the maximum processing capacity of the processing resources and the total processing resource utilization in GOPS, respectively [30], [39]. The processing resource utilization can be expressed as

$$C_{\text{cloud}} = C_{\text{proc}}^c + C_{\text{proc}}^s \quad (44)$$

where  $C_{\text{proc}}^c$  and  $C_{\text{proc}}^s$  are the processing resource utilization due to communication and sensing tasks, respectively<sup>1</sup>.

In the following parts, the required GOPS for communication and sensing in our system model is computed, respectively. We assess the computational complexity where only the numbers of real multiplications and divisions are counted. Each complex multiplication is equal to four real multiplications. We also consider memory overhead in arithmetic operation calculations by multiplying each operation by two as done in [30], [40]. Hence, each complex multiplication is counted as  $4 \cdot 2 = 8$  operations in computing the total GOPS.

##### A. GOPS Analysis of Digital Operations for Communication at the Cloud

In this section, we analyze the GOPS for digital signal processing corresponding to the communication tasks including

<sup>1</sup>In this paper, we focus on the GOPS analysis by taking into account only physical-layer communication and sensing processing and neglect high-layer operations.

the uplink channel estimation and downlink transmission. To compute the number of real multiplications, we mainly follow the GOPS analysis in [36, App. B], [17].

Let  $C_{\text{ch-est}}$  denote the computational complexity of the LMMSE channel estimation approach for all the APs. To compute the channel estimates, we first obtain the vectors  $\mathbf{y}_{t_i,k}^p$ . From [36, App. B], the multiplication of one matrix of size  $M \times L_p$  with a vector of size  $L_p \times 1$  results in  $ML_p$  complex multiplications. Hence, obtaining  $\mathbf{y}_{t_i,k}^p$  for  $N_{\text{ue}}$  UEs at all  $N_{\text{tx}}$  APs costs  $8ML_p N_{\text{ue}} N_{\text{tx}}$  real multiplications/division in total, if  $L_p \geq N_{\text{ue}}$ . Otherwise, the number of real multiplications/divisions would be  $8ML_p^2 N_{\text{tx}}$ . Moreover, we need to compute the matrices  $\mathbf{R}'_{i,k}$  and  $\mathbf{\Psi}'_{t_i,k}$ , given that  $\hat{\mathbf{h}}_{i,k}$  and  $\mathbf{R}_{i,k}$  are known. However, this pre-computation can be neglected since the channel statistics are usually constant for a while and there is no need to compute them every coherence block. Finally, the multiplications in (10) costs  $8M^2 N_{\text{ue}} N_{\text{tx}}$  real operations. Then,  $C_{\text{ch-est}}$  is equal to

$$C_{\text{ch-est}} = \begin{cases} (8ML_p + 8M^2)N_{\text{ue}}N_{\text{tx}}, & L_p \geq N_{\text{ue}} \\ 8ML_p^2 N_{\text{tx}} + 8M^2 N_{\text{ue}} N_{\text{tx}}, & L_p < N_{\text{ue}} \end{cases} \quad (45)$$

The number of real multiplications/divisions to compute centralized RZF precoding vector for all the UEs from [36, App. B] is

$$\begin{aligned} C_{\text{prec-comp}} &= \underbrace{\frac{8((MN_{\text{tx}})^2 + MN_{\text{tx}})}{2} N_{\text{ue}}}_{\text{inside the parentheses}} \\ &+ \underbrace{\frac{8((MN_{\text{tx}})^3 - MN_{\text{tx}})}{3}}_{\text{inversion}} + N_{\text{ue}} \cdot \underbrace{8(MN_{\text{tx}})^2}_{\text{for } (\cdot)^{-1} \hat{\mathbf{h}}_i} \\ &+ N_{\text{ue}} \cdot \left( \underbrace{8MN_{\text{tx}}}_{\text{computing } \|\mathbf{w}_i\|} + \underbrace{4MN_{\text{tx}}}_{\text{normalization}} \right) \\ &= (12(MN_{\text{tx}})^2 + 16MN_{\text{tx}}) N_{\text{ue}} \\ &+ \frac{8((MN_{\text{tx}})^3 - MN_{\text{tx}})}{3}. \end{aligned} \quad (46)$$

Reciprocity calibration and multiplication of the symbols by the precoding vectors, each costs  $8L_d MN_{\text{ue}} N_{\text{tx}}$  real operations [30], [41]. Multiplying by the power coefficients also costs  $4L_d MN_{\text{ue}} N_{\text{tx}}$ . Finally, the GOPS corresponding to communication processing (i.e., channel estimation, precoding and reciprocity calibration) is computed as

$$C_{\text{proc}}^c = \frac{B}{L10^9} \left( C_{\text{ch-est}} + C_{\text{prec-comp}} + 20L_d MN_{\text{ue}} N_{\text{tx}} \right), \quad (47)$$

where we divided the total giga operations by the coherence time  $L/B$ .

### B. GOPS Analysis of Digital Operations for Sensing at the Cloud

In this subsection, we present the GOPS analysis for sensing operations, including signal transmission and processing the received signal. The GOPS corresponding to the sensing

transmissions consists of computing the sensing precoding vector  $\mathbf{w}_0$ , denoted by  $C_{\text{prec-comp}}^s$ , and obtaining the sensing signal by multiplying the sensing symbols by the sensing precoding vector and the sensing power coefficient. Multiplying the sensing symbols by the sensing precoding vector and the sensing power coefficient costs  $12L_d MN_{\text{tx}}$  real multiplications/divisions. The unitary matrix  $\mathbf{U}$  in (24) (subspace spanned by the UE channel estimation vectors) is already obtained when computing the RZF precoding vectors by matrix inversion and the corresponding  $\mathbf{LDL}^H$  decomposition [36, Lem. B.2]. Therefore, the computational complexity of the ZF precoding vector  $\mathbf{w}_0$  is given by

$$C_{\text{prec-comp}}^s = 8(MN_{\text{tx}})^2 + 12MN_{\text{tx}}, \quad (48)$$

where the first term stands for matrix-vector multiplication and the second term corresponds to the cost of computing  $\|\mathbf{w}_0\|$  and normalization, which are counted as  $8MN_{\text{tx}} + 4MN_{\text{tx}}$ .

After transmitting the signal in downlink, the reflected signals along with the interference signals are received at the receiver APs and sent to the cloud. At the cloud, these signals are processed for a specific sensing application. In this work we consider target detection and assess the number of real multiplications/divisions required to compute the test statistics. For target detection problems, we usually compute the test statistics and compare them with a threshold. The target is declared detected if the value of the test statistics is greater than the threshold. We assume that the threshold is constant. Therefore, we can neglect the computational complexity of obtaining the threshold. However, test statistics should be obtained for each transmission. Hence, the sensing GOPS is obtained as

$$C_{\text{proc}}^s = \frac{B}{L10^9} \left( \underbrace{12L_d MN_{\text{tx}}}_{\text{precoding + power}} + C_{\text{prec-comp}}^s + \underbrace{C_{\text{se-comp}}}_{\text{target detection}} \right), \quad (49)$$

where  $C_{\text{se-comp}}$  denotes the computational complexity for computing the detector test statistics. Given the clutter-unaware detector in (17), the computational complexity is computed as

$$\begin{aligned} C_{\text{se-comp}}^{c\text{-unaware}} &= L_d \left( \underbrace{20MN_{\text{tx}} N_{\text{rx}}}_{\text{for } \mathbf{G}} + \underbrace{8M^2 N_{\text{rx}} N_{\text{tx}}}_{\text{for } \mathbf{a}} \right) \\ &+ \underbrace{4N_{\text{rx}} (N_{\text{tx}}^2 + N_{\text{tx}}) M}_{\text{for } \mathbf{C}} + \underbrace{8 \frac{(N_{\text{tx}}^3 - N_{\text{tx}}) N_{\text{rx}}}{3}}_{\text{for inverse } \mathbf{C}} \\ &+ \underbrace{8 \frac{((N_{\text{tx}} N_{\text{rx}})^2 + N_{\text{tx}} N_{\text{rx}})}{3}}_{\text{for final step}}, \end{aligned} \quad (50)$$

where we used the block diagonal structure of  $\mathbf{C}$  in getting the inverse of it.

The computational complexity for each step of computing the test statistics of clutter-aware detector in (18) are listed in Table I.

## VI. JOINT BLOCKLENGTH AND POWER OPTIMIZATION

In this paper, we aim to optimize the blocklength and the power control coefficients to minimize the energy consumption

TABLE I: Computational complexity with clutter-aware MAPRT detector

Operation	Computational complexity
$\mathbf{G}[m], \forall m$	$\mathcal{O}(20 L_d M N_{\text{tx}} N_{\text{rx}})$
$\mathbf{a}$	$\mathcal{O}(8 L_d M^2 N_{\text{rx}} N_{\text{tx}})$
$\mathbf{b}$	$\mathcal{O}(8 L_d M^2 N_{\text{rx}} N_{\text{tx}})$
$\mathbf{C}$	$\mathcal{O}(4 L_d M N_{\text{rx}} (N_{\text{tx}}^2 + N_{\text{tx}}))$
$\mathbf{D}$	$\mathcal{O}(4 L_d ((M N_{\text{tx}})^2 + M N_{\text{tx}}))$
$\mathbf{E}$	$\mathcal{O}(8 L_d M^2 N_{\text{rx}} N_{\text{tx}}^2)$
$\begin{bmatrix} \mathbf{C} & \mathbf{E} \\ \mathbf{E}^H & \mathbf{D} \end{bmatrix}^{-1}$	$\mathcal{O}\left(\frac{8}{3} \left( ((1 + M^2) N_{\text{tx}} N_{\text{rx}})^3 - (1 + M^2) N_{\text{tx}} N_{\text{rx}} \right)\right)$
$\mathbf{D}^{-1}$	$\mathcal{O}\left(\frac{8}{3} \left( (M^2 N_{\text{tx}} N_{\text{rx}})^3 - M^2 N_{\text{tx}} N_{\text{rx}} \right)\right)$
$\begin{bmatrix} \mathbf{a}^H & \mathbf{b}^H \end{bmatrix} \begin{bmatrix} (\cdot) \\ (\cdot) \end{bmatrix} \begin{bmatrix} \mathbf{a} \\ \mathbf{b} \end{bmatrix}$	$\mathcal{O}\left(8 \left( (1 + M^2) N_{\text{tx}} N_{\text{rx}} \right)^2 + (1 + M^2) N_{\text{tx}} N_{\text{rx}} \right)$

while URLLC and sensing requirements are satisfied. In the following subsections, we cast two non-convex optimization problems: i) minimizing only the energy consumption for transmission; ii) minimizing E2E energy consumption by taking into account the energy consumption at the radio site and the cloud.<sup>2</sup> The corresponding algorithms to these optimization problems are represented by *SeURLLC+* and *E2E SeURLLC+*, respectively.

#### A. Minimizing Energy Consumption for Transmission

The optimization problem can be cast as

$$\mathbf{P1:} \quad \underset{\rho \geq 0, L > L_p}{\text{minimize}} \quad E_{\text{tr}} = \frac{L_d}{B} P_{\text{tr}} \quad (51a)$$

$$\text{subject to} \quad \epsilon_i \leq \epsilon_i^{(\text{ub})} \leq \epsilon_i^{(\text{th})}, \quad \forall i > 0 \quad (51b)$$

$$L \leq L_{\text{max}}, \quad (51c)$$

$$\overline{\text{SINR}}_s \geq \gamma_s, \quad (51d)$$

$$P_k \leq P_{\text{tx}}, \quad k = 1, \dots, N_{\text{tx}} \quad (51e)$$

$P_{\text{tr}} = \sum_{k=1}^{N_{\text{tx}}} P_k$  is the average power consumption for transmission, given as  $P_{\text{tr}} = \sum_{j=0}^{N_{\text{ue}}} \rho_j = \|\boldsymbol{\rho}\|^2$ , where  $\boldsymbol{\rho} = [\sqrt{\rho_0} \dots \sqrt{\rho_{N_{\text{ue}}}}]^T$ , due to the unit-power centralized precoding vectors. Constraints (51b) and (51c) correspond to the URLLC requirements. The  $\gamma_s$  is the required sensing SINR that is selected according to the target detection performance requirement and  $P_{\text{tx}}$  is the maximum transmit power per AP.

The aforementioned problem is challenging to solve due to its non-convex nature and the high coupling of variables. In the following theorem, we present an equivalent optimization problem by introducing newly defined auxiliary variables. This allows us to obtain a more tractable optimization problem.

**Theorem 1.** Consider the problem in (51) and define the collective vectors  $\mathbf{r} = [r_1 \dots r_{N_{\text{ue}}}]^T$  and  $\boldsymbol{\chi} = [\chi_1 \dots \chi_{N_{\text{ue}}}]^T$ .

<sup>2</sup>In addition to considering radio and cloud processing energy consumption, it is important to take fronthaul energy consumption into account when assessing E2E energy consumption. However, in our analysis, where the primary focus is on the interplay between processing and radio resources, we treat fronthaul energy consumption as a fixed component and do not include it in our considerations.

The optimal solution  $\{\boldsymbol{\rho}^*, L^*\}$  of the problem given below is also an optimal solution to (51):

$$\underset{\rho, \boldsymbol{\chi}, \mathbf{r} \geq 0, L > L_p, \bar{L} > 0}{\text{minimize}} \quad \frac{\|\boldsymbol{\rho}\|^2}{\bar{L}} \quad (52a)$$

$$\text{subject to:} \quad L - L_p \leq \frac{1}{\bar{L}}, \quad (52b)$$

$$\ln(1 + \chi_i) - \chi_i + \frac{\rho_i \mathbf{b}_i^2}{r_i} \geq \frac{Q^{-1}(\epsilon_i^{(\text{th})})}{\sqrt{L - L_p}} + \frac{b_i \ln 2}{L - L_p} \quad (52c)$$

$$\left\| \begin{bmatrix} \sqrt{2} \mathbf{a}_{i,0} \sqrt{\rho_0} \\ \vdots \\ \sqrt{2} \mathbf{a}_{i,N_{\text{ue}}} \sqrt{\rho_{N_{\text{ue}}}} \\ \sqrt{2} \mathbf{b}_i \sqrt{\rho_i} \\ \sqrt{2} \sigma_n \\ 1 + \chi_i \\ r_i \end{bmatrix} \right\| \leq 1 + \chi_i + r_i, \forall i, \quad (52d)$$

$$\boldsymbol{\rho}^T (\gamma_s \mathbf{B}_D - M \mathbf{A}_D) \boldsymbol{\rho} \leq -\gamma_s M N_{\text{rx}} \sigma_n^2 \quad (52e)$$

$$\|\mathbf{F}_k \boldsymbol{\rho}\| \leq \sqrt{P_{\text{tx}}}, \quad k = 1, \dots, N_{\text{tx}}, \quad (52f)$$

$$L \leq L_{\text{max}}, \quad (52g)$$

where  $\mathbf{F}_k = \text{diag} \left( \sqrt{\mathbb{E}\{\|\mathbf{w}_{0,k}\|^2\}}, \dots, \sqrt{\mathbb{E}\{\|\mathbf{w}_{N_{\text{ue}},k}\|^2\}} \right)$ .

*Proof.* See Appendix A.  $\square$

The optimization problem in (52) is still not convex due to the non-convex constraints (52b), (52c) and (52e). The terms that destroy convexity are the convex terms  $1/\bar{L}$  and  $\frac{\rho_i \mathbf{b}_i^2}{r_i}$  (in terms of  $\boldsymbol{\rho}$  and  $\mathbf{r}$ ) on the right-hand side of (52b) and the left-hand side of (52c), respectively. To this end, we apply the concave-convex procedure (CCP) approach to (52b) and (52c), and the FPP-SCA method [42] to (52e), wherein  $-\boldsymbol{\rho}^T M \mathbf{A}_D \boldsymbol{\rho}$  is a concave function. Moreover, to avoid any potential infeasibility issue regarding (52e) during the initial iterations of the algorithm, we add slack variable  $\chi_0 \geq 0$  and a slack penalty  $\lambda$ , to the convexified problem at the initial iterations. In subsequent iterations, we set  $\chi_0$  to zero if it is less than a threshold, denoted as  $\chi_0 \leq \epsilon_\chi$ . Finally, the convex



problem that is solved at the  $c^{\text{th}}$  iteration becomes

$$\underset{\boldsymbol{\rho}, \boldsymbol{\chi}, \mathbf{r} \geq \mathbf{0}, L, \bar{L} > L_p, \chi_0 \geq 0}{\text{minimize}} \quad \frac{\|\boldsymbol{\rho}\|^2}{\bar{L}} + \lambda \chi_0, \quad (53a)$$

$$\text{subject to} \quad L - L_p \leq \frac{2}{\bar{L}^{(c-1)}} - \frac{\bar{L}}{\left(\bar{L}^{(c-1)}\right)^2}, \quad (53b)$$

$$\begin{aligned} \ln(1 + \chi_i) - \chi_i + 2 \frac{\sqrt{\rho_i^{(c-1)}} \mathbf{b}_i^2 \sqrt{\rho_i}}{r_i^{(c-1)}} - r_i \left( \frac{\sqrt{\rho_i^{(c-1)}} \mathbf{b}_i}{r_i^{(c-1)}} \right)^2 \\ \geq \frac{Q^{-1}(\epsilon_i^{\text{(th)}})}{\sqrt{L - L_p}} + \frac{b_i \ln 2}{L - L_p} \end{aligned} \quad (53c)$$

$$\begin{aligned} \gamma_s \boldsymbol{\rho}^T \mathbf{B}_D \boldsymbol{\rho} - 2M \Re \left( \left( \boldsymbol{\rho}^{(c-1)} \right)^T \mathbf{A}_D \boldsymbol{\rho} \right) \\ \leq -\gamma_s M N_{\text{rx}} \sigma_n^2 - M \left( \boldsymbol{\rho}^{(c-1)} \right)^T \mathbf{A}_D \boldsymbol{\rho}^{(c-1)} + \chi_0, \end{aligned} \quad (53d)$$

(52d), (52f), (52g).

The steps of FPP-SCA and CCP procedure are outlined in Algorithm 1. We empirically observed that setting  $\bar{L}^{(0)} = \frac{1}{L_{\text{max}} - L_p}$ ,  $\rho_0^{(0)} = 0$  and  $\sqrt{\rho_i^{(0)}} = 10^{-3} \sqrt{P_{\text{tx}}/N_{\text{ue}}}$  for  $i > 0$  yields satisfactory results.

---

**Algorithm 1** FPP-SCA and CCP Procedure for Problem (52).

---

- 1: **Initialization:** Set arbitrary  $\boldsymbol{\rho}^{(0)}, \mathbf{r}^{(0)} \geq \mathbf{0}$ , the solution accuracy parameters  $\epsilon, \epsilon_\chi > 0$ ,  $\bar{L}^{(0)} = \frac{1}{L_{\text{max}} - L_p}$ , and  $\lambda > 0$ . Set the iteration counter to  $c = 0$ , and a maximum iteration number  $c_{\text{max}}$ . Moreover, let  $F^{(0)} = \infty$  be the initial value of objective function and  $\Delta F^{(c)} = F^{(c)} - F^{(c-1)}$  with  $F^{(-1)} = 0$ .
  - 2:  $c \leftarrow c + 1$ .
  - 3: **While**  $\Delta F^{(c-1)} \geq \epsilon$  and  $c \leq c_{\text{max}}$ , **do**
  - 4: Set  $\boldsymbol{\rho}^{(c)}, \bar{L}^{(c)}$ , and  $\mathbf{r}^{(c)}$  to the solution of the convex problem in (53), where the previous iterates  $\boldsymbol{\rho}^{(c-1)}, \bar{L}^{(c-1)}$ , and  $\mathbf{r}^{(c-1)}$  are taken as constant.
  - 5: If  $\chi_0 < \epsilon_\chi$ , set  $\chi_0 = 0$  for the next iteration.
  - 6: **End while**
  - 7: **Output:** The transmit power coefficients  $\boldsymbol{\rho}^{(c)}$  and the blocklength  $L^{(c)}$ .
- 

### B. Minimizing E2E Energy Consumption

In this subsection, our objective is to minimize the E2E energy consumption. The optimization problem is formulated as follows

$$\begin{aligned} \mathbf{P2:} \quad & \underset{\boldsymbol{\rho} \geq \mathbf{0}, L > L_p}{\text{minimize}} \quad E_{\text{total}} = \frac{L}{B} P_{\text{total}} \\ & \text{subject to} \quad (51b), (51c), (51d), (51e). \end{aligned} \quad (54a)$$

The total power consumption can be rewritten as

$$P_{\text{total}} = P_{\text{FIXED}} + \Delta^{\text{tr}} \|\boldsymbol{\rho}\|^2 + \frac{1}{L} f_1 + \frac{L_d}{L} f_2 \quad (55)$$

where

$$P_{\text{FIXED}} = \sum_{k=1}^{N_{\text{tx}}} P_{\text{AP},0}^{\text{tx}} + \sum_{r=1}^{N_{\text{rx}}} P_{\text{AP},0}^{\text{rx}} + P_{\text{fixed}} + \frac{P_{\text{cloud},0}^{\text{proc}}}{\sigma_{\text{cool}}} \quad (56)$$

$$\begin{aligned} f_1 &= \frac{\Delta_{\text{cloud}}^{\text{proc}}}{\sigma_{\text{cool}} C_{\text{max}}} \frac{B}{10^9} \left( C_{\text{ch-est}} + C_{\text{prec-comp}} + C_{\text{prec-comp}}^{\text{S}} \right. \\ & \quad \left. + C_{\text{se-detector}} \right) \\ f_2 &= \frac{\Delta_{\text{cloud}}^{\text{proc}}}{\sigma_{\text{cool}} C_{\text{max}}} \frac{B}{10^9} (20MN_{\text{ue}}N_{\text{tx}} + 12MN_{\text{tx}} + C_{\text{se-prep},m}). \end{aligned} \quad (57)$$

(58)

Similar to the approach of problem **P1**, we define a new variable  $\bar{L}$  where  $L - L_p \leq \frac{1}{\bar{L}}$ . Then, the objective function (54a) is equivalent to

$$F_2 \triangleq \frac{1}{B} \left( L(P_{\text{FIXED}}) + (L - L_p) f_2 + \Delta^{\text{tr}} \frac{\|\boldsymbol{\rho}\|^2}{\bar{L}} \right). \quad (59)$$

The non-convex optimization problem in (54) can be solved using the same approach in **P1** as follows:

$$\begin{aligned} \underset{\boldsymbol{\rho}, \boldsymbol{\chi}, \mathbf{r} \geq \mathbf{0}, L, \bar{L} > L_p, \chi_0 \geq 0}{\text{minimize}} \quad & F_2 + \lambda \chi_0, \\ \text{subject to} \quad & (53b), (53c), (53d), (52d), (52f), (52g). \end{aligned} \quad (60a)$$

## VII. NUMERICAL RESULTS

In this section, we present numerical results to evaluate the performance of the proposed joint blocklength and power allocation algorithms. We consider a total area of  $500 \text{ m} \times 500 \text{ m}$ , with the sensing location positioned at the center. The  $N_{\text{tx}} = 16$  ISAC transmit APs are uniformly distributed in the area. We consider the number of sensing receive APs equal to  $N_{\text{rx}} = 1$  or  $N_{\text{rx}} = 2$  where the first AP is located at  $(200, 250)$  and the second one is located at  $(300, 250)$ . The number of antenna elements per AP is set to  $M = 4$ . The total number of URLLC UEs in the network is  $N_{\text{ue}} = 8$ . We set  $P_{\text{tx}} = 100 \text{ mW}$  and the uplink pilot transmission power for each UE is  $50 \text{ mW}$ .

The large-scale fading coefficients, shadowing parameters, probability of LOS, and the Rician factors are simulated based on the 3GPP Urban Microcell model, defined in [43, Table B.1.2.1-1, Table B.1.2.1-2, Table B.1.2.2.1-4]. The path losses for the Rayleigh fading target-free channels are also modeled by the 3GPP Urban Microcell model with the difference that the channel gains are multiplied by an additional scaling parameter equal to 0.3 to suppress the known parts of the target-free channels due to LOS and permanent obstacles [34]. The sensing channel gains are computed by the bi-static radar range equation [9]. The carrier frequency, the bandwidth, and the noise variance are set to 1.9 GHz, 200 KHz, and  $-114 \text{ dBm}$ , respectively. The number of pilot symbols is  $L_p = 10$ .

The spatial correlation matrices for the communication channels are generated by using the local scattering model in [35, Sec. 2.5.3]. The RCS of the target is modeled by the Swerling-I model with  $\sigma_{\text{RCS}} = 0 \text{ dBsm}$ . For all the UEs, the packet size, maximum transmission delay, and DEP threshold are  $b_i = 256 \text{ bits}$ ,  $D_i^{(\text{th})} = 1 \text{ ms}$ , and  $\epsilon_{\text{th}} = 10^{-5}$ , respectively. In the proposed algorithms,  $\epsilon = 10^{-3}$ ,  $\epsilon_\chi = 10^{-6}$ ,  $\lambda = 10$ , and  $c_{\text{max}} = 30$ . The sensing SINR threshold is set to  $\gamma_s = 0 \text{ dB}$ , unless otherwise stated. The remaining parameters are detailed in Table II, where the values are consistent with those in [30], except for a scaling of the total processing capacity

TABLE II: Simulation Parameters

$\Delta^{\text{tr}}, \sigma_{\text{cool}}$	4, 0.9	$P_{\text{fixed}}$	120 W
$P_{\text{AP},0}^{\text{tx}}, P_{\text{AP},0}^{\text{rx}}$	$6.8 \cdot M$ W, $6.8 \cdot M$ W	$P_{\text{cloud},0}^{\text{proc}}$	20.8 W
$\Delta_{\text{cloud}}^{\text{proc}}$	740 W	$C_{\text{max}}$	1800 GOPS

and the corresponding power of a DU by a factor of ten to accommodate all the processing in a single DU.

We compare the performance of two proposed algorithms: i) *SeURLLC+* aiming to minimize the transmission energy consumption, and ii) *E2E SeURLLC+* aiming to minimize the E2E energy consumption. Additionally, we include two baseline algorithms for URLLC systems without sensing integration: (i) *URLLC-only*, which minimizes transmission energy consumption, and (ii) *E2E URLLC-only*, which minimizes E2E energy consumption. We further compare results using clutter-aware and clutter-unaware MAPRT detectors, as defined in (17) and (18), respectively.

Fig. 2a illustrates the transmission energy consumption for four algorithms with the clutter-aware detector. The results show that integrating sensing into the system necessitates higher transmission energy. Notably, the *URLLC-only* and *SeURLLC+* achieve lower transmission energy compared to their E2E counterparts, as their primary objective is to minimize transmission energy consumption.

The E2E energy consumption is depicted in Fig. 2b. We observe that E2E energy minimization results in a substantial reduction in total energy consumption by approximately 50% in URLLC-only scenarios, while its impact is less pronounced in ISAC scenarios, resulting in only a marginal decrease. The E2E algorithms try to minimize the total energy consumption by reducing the blocklength. However, higher power coefficients are required to meet the reliability requirements for URLLC UEs. In *SeURLLC+*, higher power coefficients for sensing allow lower blocklength, narrowing the gap in optimal blocklengths between *SeURLLC+* and *E2E SeURLLC+*.

Fig. 2c provides a detailed breakdown of energy consumption by system components and different operations, including ISAC transmit APs, sensing receive APs, communication and sensing processing, and ‘‘Others,’’ which represent load-independent and idle mode power consumption in the cloud. For both algorithms, most of the energy consumption is attributed to sensing processing tasks, ISAC APs, and load-independent and idle mode power consumption in the cloud. However, the *E2E SeURLLC+* algorithm slightly reduces the corresponding energy consumption.

#### A. Impact of URLLC Requirements

Fig. 3 illustrates the blocklength, E2E energy consumption, detection probability and sensing update rate as functions of DEP threshold. Generally, the blocklength in Fig. 3a decreases as the reliability threshold is relaxed in all algorithms except for *URLLC-only*. The *URLLC-only* algorithm consistently uses the maximum available blocklength, i.e.,  $L_{\text{max}}$ . By integrating sensing, the optimal blocklength is significantly reduced compared to *URLLC-only*, as meeting sensing constraint requires higher power consumption resulting in lower blocklength. Relaxing the reliability constraint would generally reduce the

E2E energy consumption. However, ISAC scenarios demand higher energy consumption as it is expected as shown in Fig. 3b.

Fig. 3c and Fig. 3d demonstrate the impact of the DEP threshold on sensing performance. Relaxing the DEP constraint slightly reduces detection probability while increasing the sensing update rate, due to smaller blocklengths at higher DEP thresholds. Notably, the *E2E SeURLLC+* algorithm outperforms the *SeURLLC+* algorithm in both sensing and communication performance.

It is worth mentioning that higher delay threshold allows the system to operate with higher blocklength. However, it does not effect the results since the algorithm aims to minimize the energy consumption. Therefore, it still chooses a smaller blocklength.

#### B. Impact of Sensing Requirement

The impact of the sensing SINR threshold,  $\gamma_s$ , on the performance of the *E2E SeURLLC+* algorithm is evaluated in Figs. 4a-c in terms of E2E energy consumption, detection probability, and sensing update rate, respectively. Comparing Fig. 4a with Fig. 4b, we observe that both detection probability and energy consumption generally increase with a higher SINR threshold. The clutter-aware detector with  $N_{\text{rx}} = 2$  provides the highest detection probability, consistently above 0.9, whereas the clutter-unaware detector cannot achieve a detection probability over 0.6, despite offering the lowest energy consumption. Notably, using a clutter-aware detector while disabling one RX-AP maintains a detection probability above 0.8 with around 43% energy saving. This suggests a potential optimization strategy: turning off one sensing receive AP can halve the energy consumption, significantly enhancing overall energy efficiency. Higher sensing SINR threshold demands higher blocklength, resulting in lower sensing update rate as shown in Fig. 4c. Comparing Fig. 4b and Fig. 4c, it is evident that increasing the sensing SINR threshold significantly decreases the sensing update rate without substantially improving detection probability.

#### C. Impact of Number of APs

We explore the impact of the number of transmit and receive APs on the network performance in terms of E2E energy consumption, detection probability, and sensing update rate as shown in Figs. 5a-c, respectively. The results in Fig. 5a and Fig. 5b indicate that increasing the number of receive APs generally raises both E2E energy consumption and detection probability. For  $N_{\text{rx}} = 2$ , the detection probability substantially improves with only a marginal raise in energy consumption. However, further increasing to  $N_{\text{rx}} = 4$  offers little improvement in detection probability while significantly increasing energy consumption. Moreover, the results in Fig. 5c show a consistent sensing update rate across all curves, especially for  $N_{\text{tx}} = 8$  and  $N_{\text{tx}} = 12$ , indicating that  $N_{\text{rx}}$  has minimal impact on  $R_s$ . This suggests the optimization algorithm is more constrained by URLLC requirements than by sensing requirements.

A comparison between  $N_{\text{tx}} = 8$  and  $N_{\text{tx}} = 12$  in Fig. 5c reveals that a higher  $N_{\text{tx}}$  enhances URLLC satisfaction due

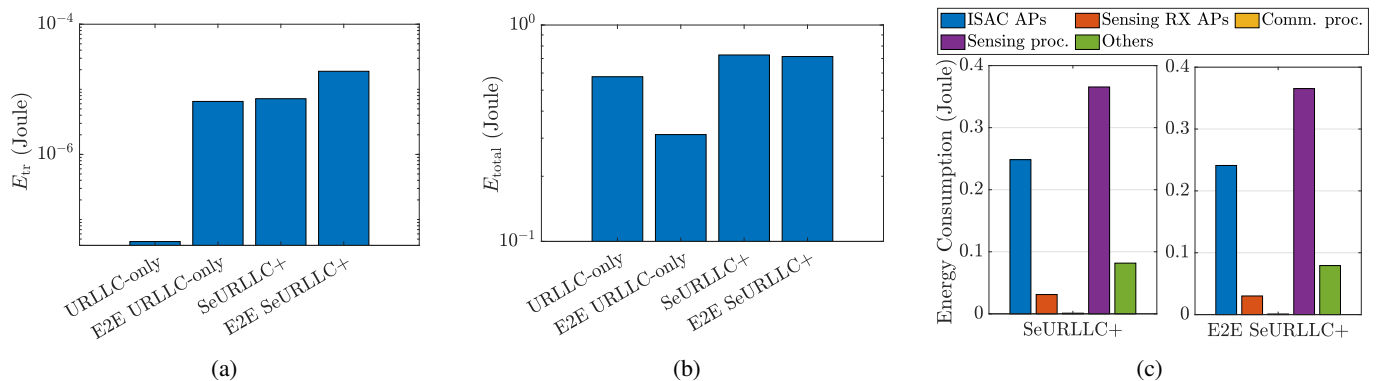


Fig. 2: (a) Transmission energy consumption, (b) E2E energy consumption, and (c) breakdown of energy consumption over one transmission for different optimization algorithms, for clutter-aware target detector with  $N_{tx} = 2$  and  $\gamma_s = 0$  dB.

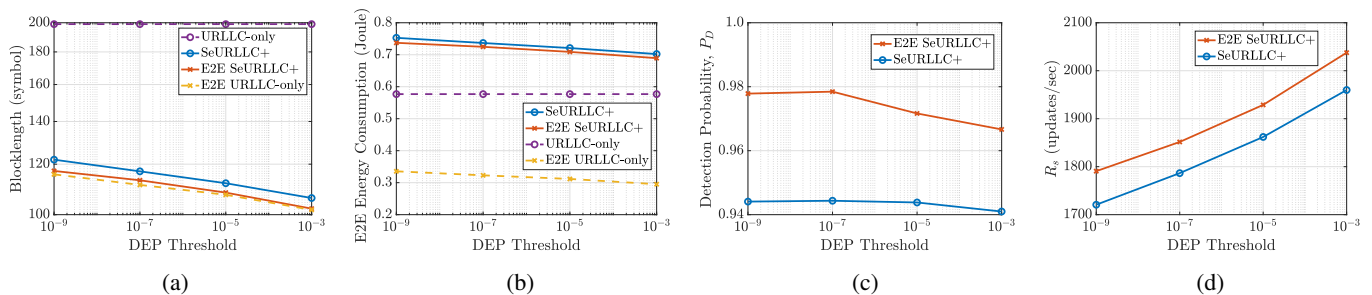


Fig. 3: (a) Blocklength, (b) E2E energy consumption, (c) detection probability, and (d) sensing update rate vs. decoding error probability threshold with clutter-aware target detector,  $N_{tx} = 2$  and  $\gamma_s = 0$  dB.

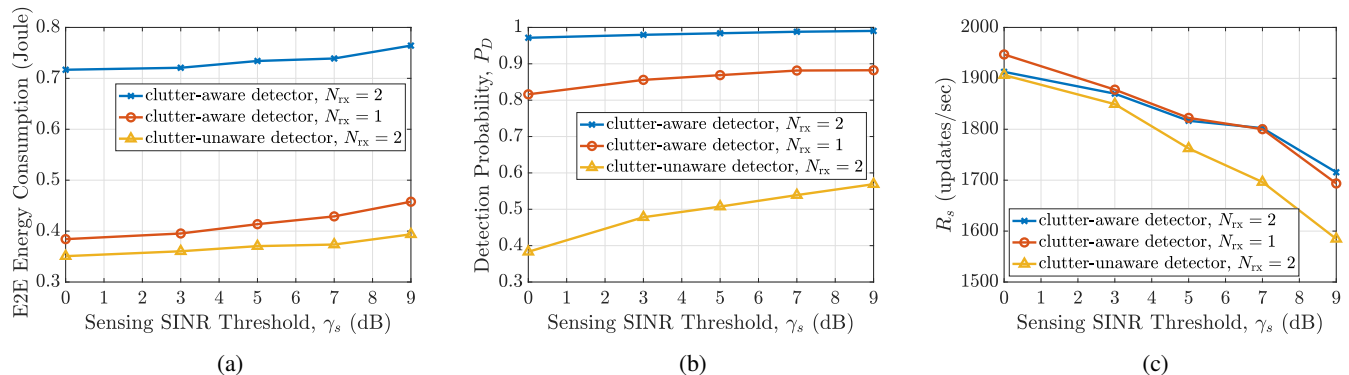


Fig. 4: (a) E2E energy consumption, (b) detection probability, and (c) sensing update rate vs. sensing SINR threshold with E2E SeURLLC+ algorithm.

to elevated SINR, resulting in a reduced blocklength and consequently a higher sensing update rate. It is observed that when  $N_{tx} = 1$  or  $N_{tx} = 2$ , increasing the number of transmit APs does not significantly affect E2E energy consumption. This is because the rise in energy consumption from the additional APs is offset by the decrease in blocklength. Thus, the overall E2E energy consumption remains relatively unchanged. Conversely, when  $N_{tx} = 4$ , the influence of  $N_{tx}$  becomes more pronounced, as the energy consumption for sensing tasks increases non-linearly with the product of  $N_{tx}$  and  $N_{rx}$ .

When  $N_{tx} = 16$ , the system's behavior concerning E2E energy consumption and detection probability follows a similar trend, showing an increase in energy consumption and a decrease in detection probability. However,  $R_s$  declines compared to when  $N_{tx} = 12$ , indicating a higher blocklength

for  $N_{tx} = 16$ . This occurs because common power coefficients are used to maintain a favorable beam pattern, and increasing the number of transmit APs may constrain power due to some APs being closer to the UEs. As a result, a higher blocklength is necessary to fulfill the reliability requirements. These findings underscore the importance of optimizing the number of transmit and receive APs.

The results of detection probability is depicted in Fig. 5b. In general, a decrease in blocklength translates to a lower detection probability explaining the results for  $N_{tx} = 12$ . However, we observe that detection probability for  $N_{tx} = 16$  still decreases although blocklength is higher compared to  $N_{tx} = 12$ . This is because the power coefficients required to satisfy the sensing SINR requirement might be lower with higher  $N_{tx}$ , resulting in a more pronounced negative impact on detection probability. This negative impact outweighs the

benefits of increased blocklength, leading to a lower detection probability.

The findings emphasize the importance of optimizing the number of transmit and receive APs to balance energy consumption, detection probability and sensing update rate. Higher numbers of transmit APs can enhance URLLC satisfaction and reduce blocklength resulting in higher sensing update rate, but must be carefully managed to avoid an unnecessary increase in energy consumption and detection probability degradation.

## VIII. CONCLUSION

In this paper, we proposed a joint blocklength and power control algorithm for a downlink CF-mMIMO system with multi-static sensing and URLLC UEs. We formulated two non-convex optimization problems focused on minimizing transmission and E2E energy consumption, and conducted GOPS analysis for both communication and sensing tasks. Numerical results demonstrated the effectiveness of the E2E energy minimization algorithm, especially in scenarios without sensing capabilities. Integrating sensing reduces the optimal blocklength compared to URLLC-only scenarios due to the higher power demands of sensing, which leads to a lower optimal blocklength. Moreover, the E2E algorithms minimize total energy consumption by further reducing the blocklength. Additionally, we observed that higher sensing SINR thresholds significantly lower the sensing update rate without substantially improving detection probability. Our findings also indicated that increasing the number of sensing receive APs raises sensing-related processing energy, suggesting that deactivating some APs can help reduce E2E energy consumption in CF-mMIMO ISAC systems. While increasing the number of transmit APs can enhance URLLC satisfaction and sensing update rate by reducing blocklength, careful management is necessary to prevent excessive energy consumption and degradation in detection probability.

## APPENDIX A PROOF OF THEOREM 1

Let us define a new optimization variable, denoted by  $\bar{L}$ , where  $L - L_p \leq 1/\bar{L}$ . Then, minimizing the objective function is equivalent to minimizing the following convex function (quadratic-over-linear function)  $\frac{\|\rho\|^2}{\bar{L}}$ . Minimizing this function, at the optimal solution, holds that  $\bar{L} = 1/L_d = 1/(L - L_p)$ . The reliability constraints in (51b) can be written in the form of

$$\ln \left( 1 + \frac{\rho_i b_i^2}{\sum_{j=0}^{N_{ue}} \rho_j a_{i,j}^2 + \sigma_n^2} \right) \geq \frac{Q^{-1}(\epsilon_i^{(th)})}{\sqrt{L - L_p}} + \frac{b_i \ln 2}{L - L_p} \quad (61)$$

according to (31), where  $\overline{\text{SINR}}_i^{(dl)}$  is substituted by (28). To handle the non-convexity of the left-hand side in (61), we define a new variable  $\chi_i$  and use fractional programming [44] to write the left-hand side as

$$\ln(1 + \chi_i) - \chi_i + (1 + \chi_i) \frac{\rho_i b_i^2}{\sum_{j=0}^{N_{ue}} \rho_j a_{i,j}^2 + \rho_i b_i^2 + \sigma_n^2}. \quad (62)$$

Moreover, to represent the upper bound to  $\left( \sum_{j=0}^{N_{ue}} \rho_j a_{i,j}^2 + \rho_i b_i^2 + \sigma_n^2 \right) / (1 + \chi_i)$ , we introduce the optimization variable  $r_i$ , similarly as in [30], for  $i = 1, \dots, N_{ue}$ , where

$$\frac{\sum_{j=0}^{N_{ue}} \rho_j a_{i,j}^2 + \rho_i b_i^2 + \sigma_n^2}{1 + \chi_i} \leq r_i, \quad (63)$$

which can be written as a second-order cone (SOC) constraint in (52d). We then re-cast the constraint in (62) as

$$\ln(1 + \chi_i) - \chi_i + \frac{\rho_i b_i^2}{r_i} \geq \frac{Q^{-1}(\epsilon_i^{(th)})}{\sqrt{L - L_p}} + \frac{b_i \ln 2}{L - L_p} \quad (64)$$

which will not destroy optimality since we want to minimize  $r_i$  to increase the left-hand side of the SINR constraint.

From (38), the sensing constraint in (51d) are expressed as

$$\rho^T (\gamma_s \mathbf{B}_D - M \mathbf{A}_D) \rho \leq -\gamma_s M N_{tx} \sigma_n^2. \quad (65)$$

Finally, we define  $\mathbf{F}_k = \text{diag} \left( \sqrt{\mathbb{E} \{\|\mathbf{w}_{0,k}\|^2\}}, \dots, \sqrt{\mathbb{E} \{\|\mathbf{w}_{N_{ue},k}\|^2\}} \right)$  and rewrite the per-AP power constraints in (51e) in SOC form in terms of  $\rho$  as  $\|\mathbf{F}_k \rho\| \leq \sqrt{P_{tx}}$ , for  $k = 1, \dots, N_{tx}$ .

## REFERENCES

- [1] F. Liu, Y. Cui, C. Masouros, J. Xu, T. X. Han, Y. C. Eldar, and S. Buzzi, "Integrated sensing and communications: Towards dual-functional wireless networks for 6G and beyond," *IEEE J. Sel. Areas Commun.*, 2022.
- [2] W. Zhou, R. Zhang, G. Chen, and W. Wu, "Integrated sensing and communication waveform design: A survey," *IEEE Open J. Commun. Soc.*, vol. 3, pp. 1930–1949, 2022.
- [3] F. Salehi, M. Ozger, and C. Cavdar, "Reliability and delay analysis of 3-Dimensional networks with multi-connectivity: Satellite, HAPs, and cellular communications," *IEEE Transactions on Network and Service Management*, pp. 1–1, 2023.
- [4] Q. Peng, H. Ren, C. Pan, N. Liu, and M. ElKashlan, "Resource allocation for cell-free massive MIMO-enabled URLLC downlink systems," *IEEE Transactions on Vehicular Technology*, 2023.
- [5] C. Ding, C. Zeng, C. Chang, J.-B. Wang, and M. Lin, "Joint precoding for MIMO radar and URLLC in ISAC systems," in *Proceedings of the 1st ACM MobiCom Workshop on Integrated Sensing and Communications Systems*, 2022, pp. 12–18.
- [6] M. Ozger, M. Vondra, and C. Cavdar, "Towards beyond visual line of sight piloting of UAVs with ultra reliable low latency communication," in *2018 IEEE Global Communications Conference (GLOBECOM)*, 2018, pp. 1–6.
- [7] C. Sun, C. She, C. Yang, T. Q. Quek, Y. Li, and B. Vucetic, "Optimizing resource allocation in the short blocklength regime for ultra-reliable and low-latency communications," *IEEE Trans. Wirel. Commun.*, vol. 18, no. 1, pp. 402–415, 2018.
- [8] A. Lancho, G. Durisi, and L. Sanguinetti, "Cell-free massive MIMO for URLLC: A finite-blocklength analysis," *IEEE Trans. Wirel. Commun.*, 2023.
- [9] M. A. Richards, J. Scheer, and W. A. Holm, *Principles of Modern Radar: Basic Principles*. New York, NY, USA: Scitech, 2010.
- [10] H. Ren, C. Pan, Y. Deng, M. ElKashlan, and A. Nallanathan, "Joint pilot and payload power allocation for massive-MIMO-enabled URLLC IIoT networks," *IEEE J. Sel. Areas Commun.*, vol. 38, no. 5, pp. 816–830, 2020.
- [11] A. A. Nasir, H. D. Tuan, H. Q. Ngo, T. Q. Duong, and H. V. Poor, "Cell-free massive MIMO in the short blocklength regime for URLLC," *IEEE Transactions on Wireless Communications*, vol. 20, no. 9, pp. 5861–5871, 2021.
- [12] A. Sakhnini, M. Guenach, A. Bourdoux, H. Sahli, and S. Pollin, "A target detection analysis in cell-free massive MIMO joint communication and radar systems," in *IEEE ICC*, 2022, pp. 2567–2572.
- [13] Z. Behdad, Ö. T. Demir, K. W. Sung, E. Björnson, and C. Cavdar, "Power allocation for joint communication and sensing in cell-free massive MIMO," in *IEEE Glob. Commun. Conf.*, 2022, pp. 4081–4086.

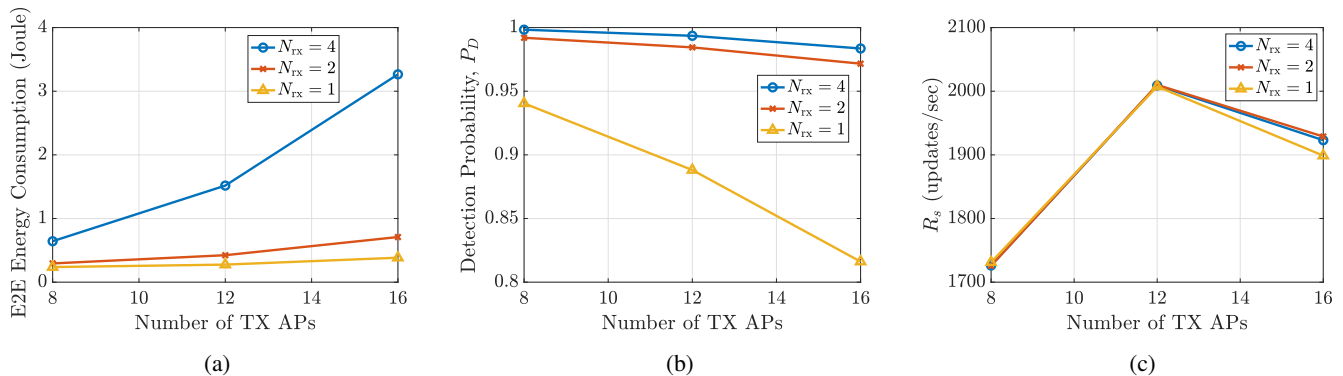


Fig. 5: (a) E2E energy consumption, (b) detection probability, and (c) sensing update rate vs. the number of transmit ISAC APs for  $N_{rx} = 1, 2, 4$  and E2E SeURLLC+ algorithm.

- [14] U. Demirhan and A. Alkhateeb, "Cell-free ISAC MIMO systems: Joint sensing and communication beamforming," *arXiv preprint arXiv:2301.11328*, 2023.
- [15] S. Buzzi, C. D'Andrea, and S. Liesegang, "Scalability and implementation aspects of cell-free massive MIMO for ISAC," *arXiv preprint arXiv:2404.14874*, 2024.
- [16] D. Wang, C. Zhang, Y. Du, J. Zhao, M. Jiang, and X. You, "Implementation of a cloud-based cell-free distributed massive MIMO system," *IEEE Communications Magazine*, vol. 58, no. 8, pp. 61–67, 2020.
- [17] Ö. T. Demir, M. Masoudi, E. Björnson, and C. Cavdar, "Cell-free massive MIMO in virtualized CRAN: How to minimize the total network power?" in *IEEE ICC*, 2022.
- [18] A. A. Nasir, H. D. Tuan, H. H. Nguyen, M. Debbah, and H. V. Poor, "Resource allocation and beamforming design in the short blocklength regime for URLLC," *IEEE Transactions on Wireless Communications*, vol. 20, no. 2, pp. 1321–1335, 2020.
- [19] M. Soleymani, I. Santamaria, E. Jorswieck, and B. Clerckx, "Optimization of rate-splitting multiple access in beyond diagonal RIS-assisted URLLC systems," *IEEE Transactions on Wireless Communications*, 2023.
- [20] D. Van Huynh, V.-D. Nguyen, S. Chatzinotas, S. R. Khoravirad, H. V. Poor, and T. Q. Duong, "Joint communication and computation offloading for ultra-reliable and low-latency with multi-tier computing," *IEEE Journal on Selected Areas in Communications*, vol. 41, no. 2, pp. 521–537, 2022.
- [21] A. Lancho, G. Durisi, and L. Sanguinetti, "Cell-free massive MIMO with short packets," in *2021 IEEE 22nd International Workshop on Signal Processing Advances in Wireless Communications (SPAWC)*. IEEE, 2021, pp. 416–420.
- [22] J. Östman, A. Lancho, G. Durisi, and L. Sanguinetti, "URLLC with massive MIMO: Analysis and design at finite blocklength," *IEEE Transactions on Wireless Communications*, vol. 20, no. 10, pp. 6387–6401, 2021.
- [23] M. Alonzo, P. Baracca, S. R. Khoravirad, and S. Buzzi, "Cell-free and user-centric massive MIMO architectures for reliable communications in indoor factory environments," *IEEE Open Journal of the Communications Society*, vol. 2, pp. 1390–1404, 2021.
- [24] M. Elwekeil, A. Zappone, and S. Buzzi, "Power control in cell-free massive MIMO networks for UAVs URLLC under the finite blocklength regime," *IEEE Transactions on Communications*, vol. 71, no. 2, pp. 1126–1140, 2022.
- [25] H. Ren, C. Pan, Y. Deng, M. Elkhshlan, and A. Nallanathan, "Joint power and blocklength optimization for URLLC in a factory automation scenario," *IEEE Transactions on Wireless Communications*, vol. 19, no. 3, pp. 1786–1801, 2019.
- [26] L. Yang, J. Jia, J. Chen, and X. Wang, "Joint power allocation and blocklength assignment for reliability optimization in CA-enabled HetNets," *Peer-to-Peer Networking and Applications*, vol. 17, no. 1, pp. 358–372, 2024.
- [27] X. Zhao and Y.-J. A. Zhang, "Joint beamforming and scheduling for integrated sensing and communication systems in URLLC," in *IEEE Glob. Commun. Conf.*, 2022, pp. 3611–3616.
- [28] A. Alabbasi, X. Wang, and C. Cavdar, "Optimal processing allocation to minimize energy and bandwidth consumption in hybrid CRAN," *IEEE Transactions on Green Communications and Networking*, vol. 2, no. 2, pp. 545–555, 2018.
- [29] M. Masoudi, Ö. T. Demir, J. Zander, and C. Cavdar, "Energy-optimal end-to-end network slicing in cloud-based architecture," *IEEE Open Journal of the Communications Society*, vol. 3, pp. 574–592, 2022.
- [30] Ö. T. Demir, M. Masoudi, E. Björnson, and C. Cavdar, "Cell-free massive MIMO in O-RAN: Energy-aware joint orchestration of cloud, fronthaul, and radio resources," *IEEE Journal on Selected Areas in Communications*, 2024.
- [31] Z. Yang, C. Pan, J. Hou, and M. Shikh-Bahaei, "Efficient resource allocation for mobile-edge computing networks with NOMA: Completion time and energy minimization," *IEEE Transactions on Communications*, vol. 67, no. 11, pp. 7771–7784, 2019.
- [32] Y. Cao and Q.-Y. Yu, "Joint resource allocation for user-centric cell-free integrated sensing and communication systems," *IEEE Communications Letters*, 2023.
- [33] Z. Behdad, Ö. T. Demir, K. W. Sung, and C. Cavdar, "Interplay between sensing and communication in cell-free massive MIMO with URLLC users," *IEEE Wireless Communications and Networking Conference (WCNC)*, 2024.
- [34] Z. Behdad, Ö. T. Demir, K. W. Sung, E. Björnson, and C. Cavdar, "Multi-static target detection and power allocation for integrated sensing and communication in cell-free massive MIMO," to appear in *IEEE Trans. Wirel. Commun.*, 2024.
- [35] Ö. T. Demir, E. Björnson, and L. Sanguinetti, "Foundations of user-centric cell-free massive MIMO," *Found. Trends Signal Process.*, vol. 14, no. 3-4, pp. 162–472, 2021.
- [36] E. Björnson, J. Hoydis, and L. Sanguinetti, "Massive MIMO networks: Spectral, energy, and hardware efficiency," *Foundations and Trends® in Signal Processing*, vol. 11, no. 3-4, pp. 154–655, 2017.
- [37] Z. Wang, J. Zhang, E. Björnson, and B. Ai, "Uplink performance of cell-free massive MIMO over spatially correlated Rician fading channels," *IEEE Communications Letters*, vol. 25, no. 4, pp. 1348–1352, 2020.
- [38] D. Shiu, G. Foschini, M. Gans, and J. Kahn, "Fading correlation and its effect on the capacity of multielement antenna systems," *IEEE Trans. Commun.*, vol. 48, no. 3, pp. 502–513, 2000.
- [39] M. Masoudi, S. S. Lisi, and C. Cavdar, "Cost-effective migration toward virtualized C-RAN with scalable fronthaul design," *IEEE Systems Journal*, vol. 14, no. 4, pp. 5100–5110, 2020.
- [40] C. Desset and B. Debaillie, "Massive MIMO for energy-efficient communications," in *2016 46th European Microwave Conference (EuMC)*. IEEE, 2016, pp. 138–141.
- [41] S. Malkowsky, J. Vieira, L. Liu, P. Harris, K. Nieman, N. Kundargi, I. C. Wong, F. Tufvesson, V. Öwall, and O. Edfors, "The world's first real-time testbed for massive MIMO: Design, implementation, and validation," *IEEE Access*, vol. 5, pp. 9073–9088, 2017.
- [42] O. Mehanha, K. Huang, B. Gopalakrishnan, A. Konar, and N. D. Sidiropoulos, "Feasible point pursuit and successive approximation of non-convex QCQPs," *IEEE Signal Process Lett.*, vol. 22, no. 7, pp. 804–808, 2014.
- [43] 3GPP, "Further advancements for E-UTRA physical layer aspects (release 9)," *TS 36.814*, 2017.
- [44] K. Shen and W. Yu, "Fractional programming for communication systems—part II: Uplink scheduling via matching," *IEEE Transactions on Signal Processing*, vol. 66, no. 10, pp. 2631–2644, 2018.